Chemical Geology 695 (2025) 123031

Contents lists available at ScienceDirect

Chemical Geology

journal homepage: www.elsevier.com/locate/chemgeo

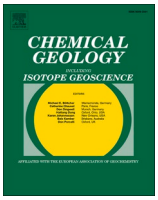

Research paper

# Flash vaporization and migration of iodine in the oceanic plate subduction zone

Noriyuki Suzuki [a,*], Jun Kameda [b], Miki Amo [c]

[a] Department of Earth and Planetary Sciences, Faculty of Science, Hokkaido University; Kita-ku, N10 W8, Sapporo 060-0810, Japan
[b] Institute for Planetary Materials, Okayama University; 827 Yamada, Misasa, Tottori 682-0193, Japan
[c] Geology and Geophysics Division, Technology Department, Japan Organization for Metals and Energy Security; 1-2-2 Hamada, Mihama-ku, Chiba 261-0025, Japan

ARTICLE INFO

Editor: Dr. Claudia Romano

*Keywords:*
Iodine circulation
Flash vaporization
Microbial methane
Thermogenic methane
Thermogenic hydrogen
Subducted sediments

ABSTRACT

Crustal fluids in subduction zones, such as subsurface aquifers, submarine seeps, and gas hydrate waters, are often rich in iodine ($I_2$) and methane ($CH_4$). Large-scale aquifers in the Kanto subduction zone, where the Pacific Plate (PAC) and the Philippine Sea Plate (PHS) are subducting, also exhibit high concentrations of $I_2$ and $CH_4$. However, the origin and behavior of $I_2$ in the subduction zone are unclear, and its coexistence with $CH_4$ remains unresolved. To investigate this, we compiled the $I_2$ phase diagram under high-pressure and high-temperature (P–T) conditions to predict its physicochemical properties in the subduction zone. We then applied the P–T paths of subducted PAC and PHS sediments to the $I_2$ phase diagram. Our findings reveal that $I_2$ can exist as a liquid in the young and hot PHS subduction zone. Transient decompressions during earthquake ruptures can cause liquid iodine to flash-vaporize and be expelled from subducted sediments. Along with $I_2$, thermogenic $CH_4$ and hydrogen ($H_2$) generated in the subducted sediments are also released and transported upward, likely by slab-dehydrated fluids. Additionally, $H_2$ may enhance microbial $CH_4$ production through hydrogenotrophic methanogenesis. In subduction zones of young and hot oceanic plates such as the PHS, crustal fluids are enriched in $I_2$ and coexist with $CH_4$ owing to the simultaneous expulsion of $I_2$, $CH_4$, and $H_2$ from the same subducted sediments and their migration via deep fluids. Large subsurface aquifers can act as traps and reservoirs for migrating $I_2$ and $CH_4$, forming large-scale $I_2$ and $CH_4$ deposits.

## 1. Introduction

Iodine in marine sediments primarily originates from marine algae and is deposited alongside algal remains (Tsunogai and Henmi, 1971; Price and Calvert, 1977; Harvey, 1980). Owing to its strong affinity for organic matter, iodine tends to accumulate in marine shales with high total organic carbon (TOC) content (Cosgrove, 1970; Muramatsu and Wedepohl, 1998; Morane et al., 1998). It is released along with petroleum from marine source rocks and migrates into reservoir rocks, leading to brine water enriched in dissolved iodine (Tomaru et al., 2009; Fehn, 2012). However, large-scale dissolved iodine deposits have also formed in the non-petroliferous Kanto Basin, indicating that iodine accumulation can occur independently of oil migration from marine source rocks. The aquifers of the Kanto Basin contain highly concentrated dissolved iodine, accounting for approximately 20 % of the world's annual iodine production (Schnebele, 2024; JNGA (Japan Natural Gas Association), 2024). These aquifers are also rich in methane ($CH_4$), forming the South Kanto natural gas fields (Sawaki et al., 2016). Similar iodine enrichment has been observed in gas hydrate waters in subduction zones, including the Nankai Trough (Fehn et al., 2003; Tomaru et al., 2007), Cascadia Margin (Fehn et al., 2006), Peru Margin (Fehn et al., 2007), and Costa Rica Margin (Fehn, 2012). Additionally, crustal fluids such as $CH_4$-rich submarine seeps in subduction zones are often found to contain high concentrations of iodine (Muramatsu and Wedepohl, 1998; Fehn, 2012). However, the origin and behavior of iodine in the subduction zones and why it coexists with $CH_4$ remain unresolved.

The Kanto Basin is a key location for investigating iodine-related processes in subduction zones because it hosts large-scale aquifers where highly concentrated dissolved iodine and $CH_4$ coexist. This region is uniquely influenced by the subduction of both the old, cold Pacific Plate (PAC) and the young, hot Philippine Sea Plate (PHS) (Fig. 1). Comprising sedimentary rocks with generally low TOC content—typically less than 1 % (Koma et al., 1983; Yonetani et al., 1983)—the Kanto

* Corresponding author.
*E-mail addresses:* suzu@y2.dion.ne.jp (N. Suzuki), jkameda@okayama-u.ac.jp (J. Kameda), amo-miki@jogmec.go.jp (M. Amo).

https://doi.org/10.1016/j.chemgeo.2025.123031
Received 7 May 2025; Received in revised form 29 August 2025; Accepted 2 September 2025
Available online 3 September 2025

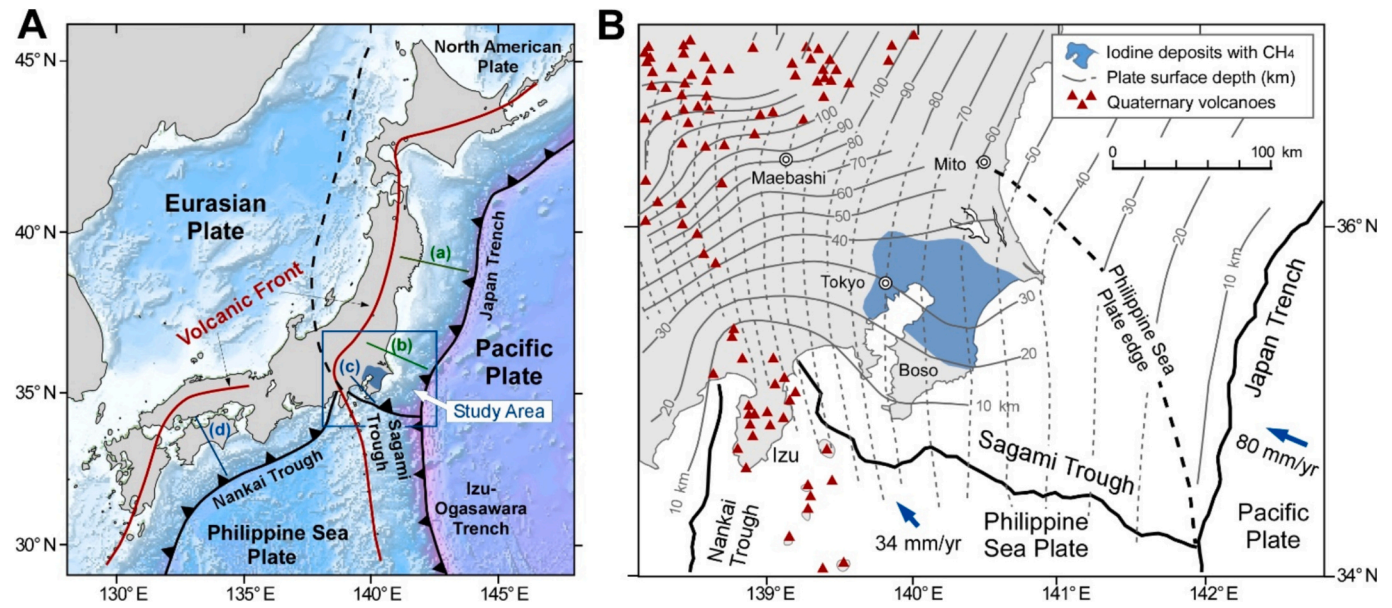


**Fig. 1.** Location of the South Kanto gas field with iodine deposits. (A) Location of the study area and selected sites along the PAC and PHS sections: (a) Sanriku, (b) North Kanto, (c) South Kanto, and (d) Shikoku. The sea bottom topographic map is provided by the Marine Information Research Center, Japan. (B) Location of the South Kanto gas field with iodine deposits (Sawaki et al., 2016). The plate surface depths of the PAC and PHS, the PHS edge, the distribution of Quaternary volcanoes, and the plate subduction rates are obtained from Wada and He (2017) and the Geological Survey of Japan, AIST (2023).

Basin is a Neogene forearc basin located near the triple junction of the PAC, PHS, and North American Plate. The iodine-rich aquifers containing $CH_4$ are located in the Late Pliocene to Pleistocene Kazusa Group, at depths of 200–1000 m below the surface. $^{129}I$ dating of the dissolved iodine suggests a geological age of approximately 50 Myr—considerably older than the sedimentary rocks of the Kanto Basin and the PHS. This has led to the hypothesis that marine sediments subducting with the PAC served as the source rocks for the iodine deposits (Muramatsu et al., 2001). However, the validity of $^{129}I$ dating is currently under debate (Ohta et al., 2024). The mechanisms by which iodine is expelled from organic-poor source rocks, migrates, and accumulates in aquifers alongside $CH_4$ remain unclear.

To better understand iodine behavior in subduction zones, we focused on its physicochemical properties as a sublime substance. Using the phase equilibrium diagram of iodine, we can predict its behavior under high-pressure and high-temperature (P–T) conditions. However, a phase diagram applicable to deep subsurface conditions in subduction zones is not currently available. In this study, we compile an iodine phase diagram for high P–T conditions in subduction zones by combining published laboratory experimental data and empirical equations. We apply the P–T paths of oceanic sediments subducting with the PAC and PHS to the iodine phase diagram to predict iodine's physicochemical properties in the subduction zone.

The considerably higher plate subduction rate compared to that of sedimentary basins leads to the generation and expulsion of substantial amounts of thermogenic $CH_4$ and hydrogen ($H_2$) from subducted sediments. This process contributes to seafloor $CH_4$ emissions and the formation of gas hydrates (Suzuki et al., 2024). Understanding the behavior of iodine, thermogenic $CH_4$, and $H_2$ in subduction zones can provide valuable insights into the mechanisms behind the accumulation and coexistence of iodine and $CH_4$ in the aquifers of the Kanto Basin, as well as in gas hydrate waters and other crustal fluids in subduction zones. In this study, we predict the physicochemical properties of iodine under varying P–T conditions in subduction zones to examine its vaporization and expulsion during rock ruptures caused by interplate earthquakes. Additionally, we explore the activity and role of slab-dehydrated fluids in the migration and accumulation of iodine, $CH_4$, and $H_2$ in subduction zones.

## 2. Methods

### 2.1. Phase diagram of iodine under high pressure and temperature

The melting, boiling, and triple points of molecular iodine ($I_2$) have been determined with sufficient accuracy (Pavese, 2022). However, a phase diagram for $I_2$ under high P–T conditions, which is essential for predicting its behavior in subduction zones, is not currently available. In this study, we compiled a phase diagram for $I_2$ in P–T ranges of 0.01–3000 MPa and 0 °C–700 °C, using available data on its melting and vapor pressure curves. The melting curves of $I_2$ in the pressure range of 0–250 MPa and 1500–4000 MPa have been obtained through laboratory experiments (Babb Jr., 1969; Brazhkin et al., 1999) (Table S1). The melting curve between 250 and 1500 MPa was estimated by extrapolating the curves above 250 MPa and below 1500 MPa, using Simon's equation.

$$P = A\left[\left(\frac{T}{T_o}\right)^{C} - 1\right] \tag{1}$$

where $P$ is the pressure, $T$ is the temperature (K), $T_o$ (=386.8 K) is the melting point at $P = 0$, and A and C are fitting constants. The constants for Simon's equation in the pressure ranges below 250 MPa and between 1500 and 3000 MPa are A = 467 and C = 2.74, and A = 391 and C = 2.60, respectively (Babb Jr., 1969; Brazhkin et al., 1999). The melting curves between 250 and 1500 MPa can be extrapolated from Simon's equation using these constants (Table S1). The melting curve between 250 and 1500 MPa can be drawn based on the extrapolated curves above 250 MPa and below 1500 MPa. By compiling these melting curves and the triple point at 0.012 MPa and 113.3 °C, we can establish a complete dataset and obtain the melting curve from 0.01 to 4000 MPa (Table S1).

The vapor pressure curve of $I_2$ was estimated using the Antoine equation, considering the triple point and the critical point at 11.7 MPa and 546 °C.

$$\log_{10}(P) = A - \frac{B}{T + C} \tag{2}$$

where $P$ represents the pressure (mmHg = 133.322 Pa), $T$ is the

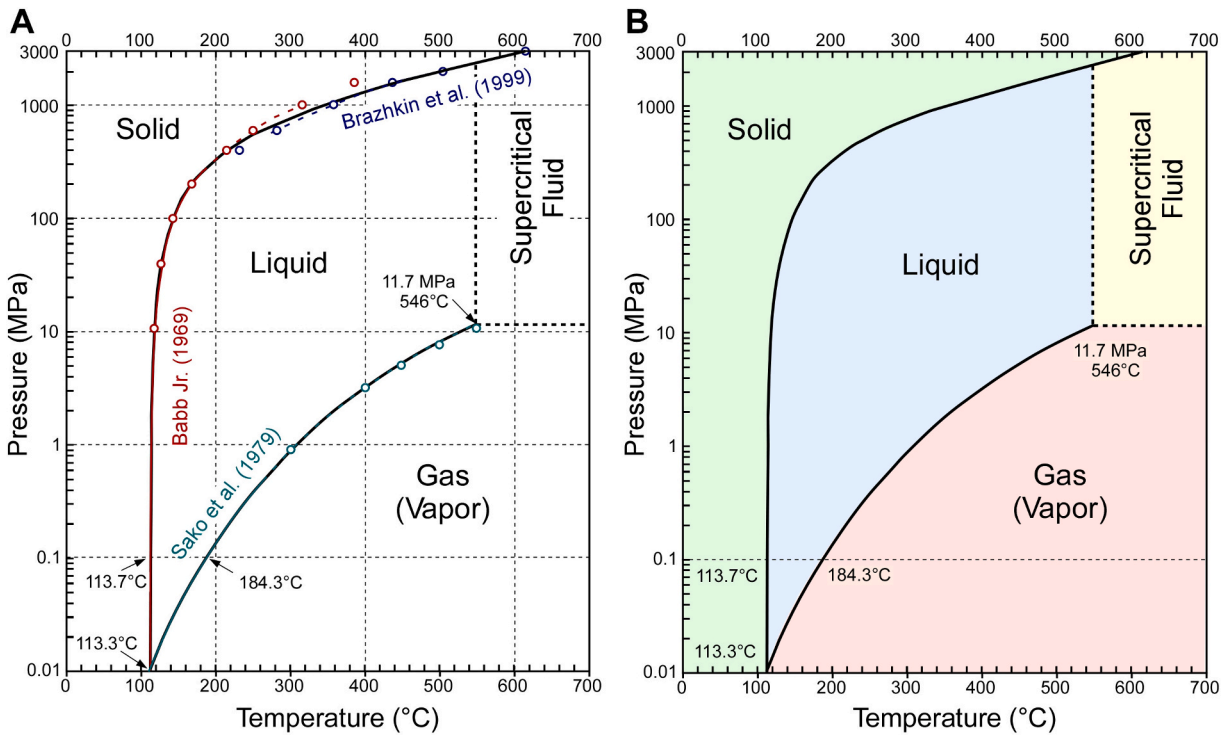


**Fig. 2.** Phase diagram of iodine under high P–T conditions. (A) Extrapolated melting and vapor pressure curves of $I_2$. (B) The phase diagram of $I_2$. The P–T conditions of the triple point, normal melting and boiling points, and the supercritical fluid are obtained from Pavese (2022). The melting curve for $I_2$ below 250 MPa and above 1500 MPa is from Babb Jr. (1969) and Brazhkin et al. (1999), respectively. The melting curve between 250 and 1500 MPa is extrapolated using Simon's equation (Table S1). The vapor pressure (defining the boundary between liquid and gas) from 0.013 to 0.51 MPa (temperature range of 116 °C–263 °C) is from Sako et al. (1979). The vapor pressure from 0.5 to 10 MPa was extrapolated from the Antoine equation (Table S2).

temperature (°C), and A, B, and C are fitting constants. Based on experiments measuring the vapor pressure of liquid $I_2$, the constants A, B, and C of the Antoine equation in the P–T range of 0.013–0.51 MPa and 116.2 °C–263.2 °C were estimated to be 7.123438, 1694.23, and 214.83, respectively (Sako et al., 1979). The vapor pressure curve from 300 °C to 546 °C (the critical point temperature) was extrapolated using the constants from Sako et al. (1979) (Table S2).

### 2.2. Decompression by flash vaporization during earthquakes

Decompression in the earthquake rupture area was estimated using the simple piston model (Weatherley and Henley, 2013), which relates the volume change in the fault jog to the earthquake moment magnitude, $M_w$. By applying updated empirical scaling relations for small-magnitude ($M_w < 5$) strike–slip earthquakes with epicenter depths ranging from 3.5 to 45 km (Leonard, 2014; Sanchez-Alfaro et al., 2016), the rupture length ($L$) can be expressed as:

$$\log_{10}L = \frac{M_w + 10.7 \times 1.5 - 14.862}{2.5} \tag{3}$$

The down-dip width ($W$) of the rupture is calculated using established empirical relationships: $W = L$ for small-magnitude earthquakes ($M_w < 5$); $W = 15.0\ L^{2/3}$ for moderate earthquakes ($5 < M_w < 6.5$); and $W = 17$ km, the average crustal seismogenic width, for large earthquakes ($M_w > 6.5$) (Weatherley and Henley, 2013).

The average slip ($s$) and the relative volume change ($\Delta V$) are calculated using the following equations (Weatherley and Henley, 2013):

$$\log_{10}s = 0.833\log_{10}L - 3.84 \tag{4}$$

$$\frac{V_f}{V_i} = \frac{V_i + \Delta V}{V_i} = 1 + \frac{s}{d} \tag{5}$$

$$\Delta V = WDs \tag{6}$$

where the down-dip width is assumed to be equal to the vertical extent of the jog. $D$ represents the step-over distance (or jog length), and it is assumed that $D \approx 1$ m for subsequent calculations. $d$ denotes the initial effective aperture thickness, where $d \approx 100$ μm. $V_i$ and $V_f$ are the initial and final volumes of the jog, respectively. Estimates for rupture length, rupture width, average slip, and relative volume change for various earthquake magnitudes are provided in Table S3. In this model, volume expansion is considered isothermal at the scale of the jog and its surrounding area (Weatherley and Henley, 2013). Under isothermal expansion at a specified temperature, the relative pressure change is given:

$$\frac{P_f}{P_i} = \frac{V_i}{V_f} = \frac{1}{1 + \frac{s}{d}} \tag{7}$$

where $P_i$ and $P_f$ are the initial and final pressures of the jog, respectively.

## 3. Results and discussion

### 3.1. Iodine phase diagram for subducted sediments

Marine sediments are subducting deeply with the PAC and PHS along the plate boundary beneath the megathrust (décollement) in the Kanto subduction zone. These underthrust sediments consist of pelagic sediments deposited on the oceanic crust, as well as marine and terrestrial sediments deposited in the trench. While the organic matter and lithologies of the underthrust sediments are diverse and not fully understood, the average TOC concentration is estimated to be approximately 0.5 wt% (Raimbourg et al., 2017). Oil expulsion does not occur sufficiently in organic-poor sedimentary rocks owing to the insufficient development of the oil network due to limited oil generation (Ungerer,

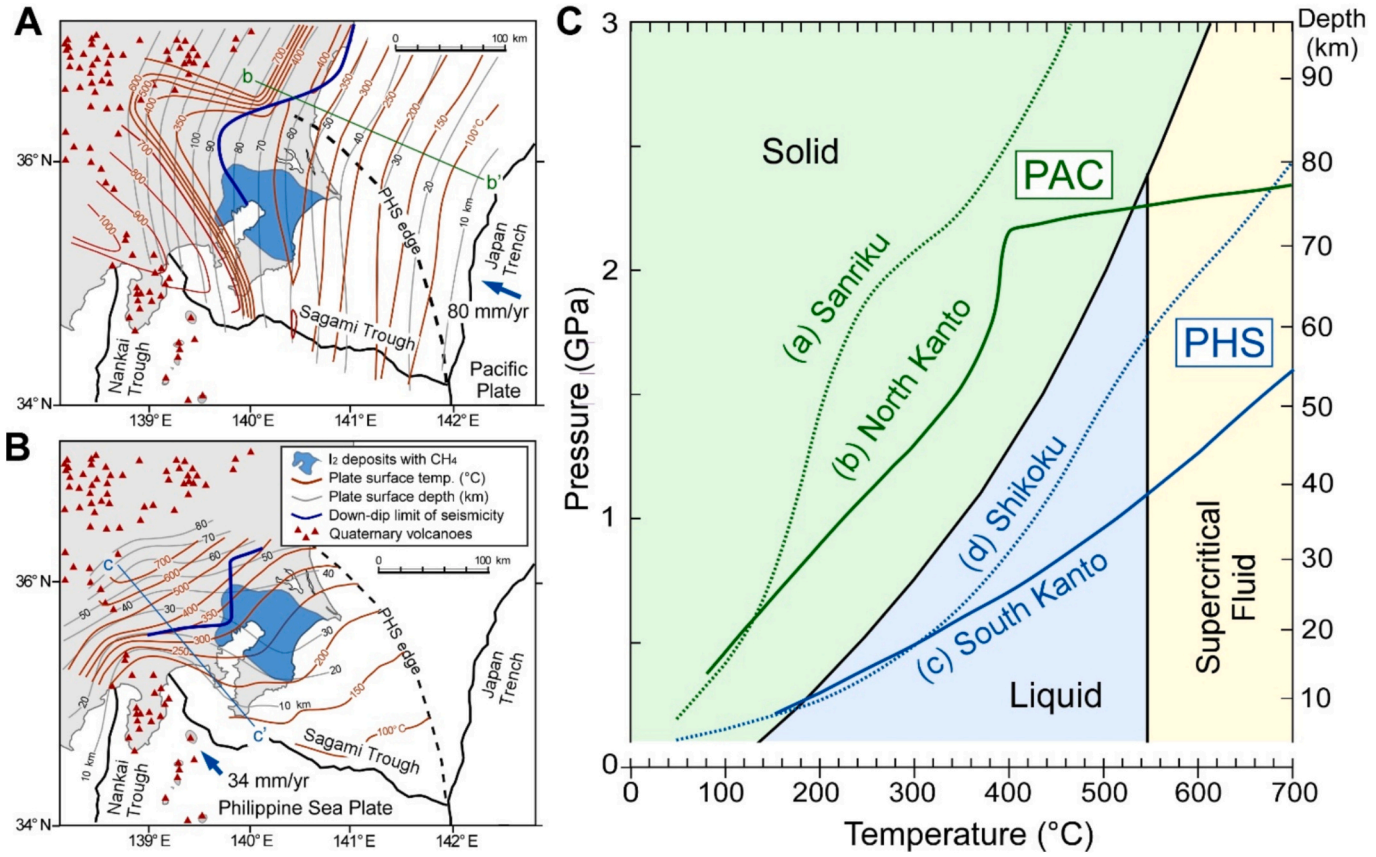


**Fig. 3.** Thermal structure of the Kanto subduction zone and the P–T paths of the PAC and PHS on the $I_2$ phase diagram. Surface temperatures and depths of the (A) PAC and (B) PHS plates in the Kanto subduction zone (Wada and He, 2017). The edge of the PHS, the distribution of Quaternary volcanoes, and the plate subduction rates are obtained from Wada and He (2017) and the Geological Survey of Japan, AIST (2023). (C) The P–T paths of the PAC and PHS surfaces in (a) Sanriku, (b) North Kanto, (c) South Kanto, and (d) Shikoku on the $I_2$ phase diagram. The locations of (a)–(d) are shown in Fig. 1A. The P–T paths for (a) and (d) are from Peacock and Wang (1999), while those for (b) and (c) are obtained from sections b–b' and c–c' in A and B, respectively.

1990; Pepper, 1991). As a result, most iodine, which has an affinity for organic matter, is retained in the underthrust sediments, where it undergoes metagenesis and metamorphism.

Iodine in the pore water of sedimentary rocks under reducing conditions exists as dissolved molecular iodine ($I_2$), iodide ($I^-$), and triiodide ($I_3^-$) (Fuge and Johnson, 1986; Fuge, 2013). They are strong nucleophiles (electron donors) and can form bonds with polar functional groups containing heteroatoms, such as oxygen. However, because the functional groups that react with iodine are no longer present in kerogen by the dry gas generation stage (Tissot and Welte, 2013), organic iodine is likely very poor in the metagenesis to metamorphism stages. Since the ionic radius of iodine is large (220 pm), it is unlikely that any minerals would readily accept iodine anions for element substitutions during diagenesis and metamorphism (Fuge and Johnson, 1986). Authigenic minerals containing iodine anions have been scarcely found in sedimentary rocks that have undergone sediment diagenesis under reducing conditions. Furthermore, $I^-$ easily loses an electron to form $I_2$, owing to its weak electron affinity (Fuge and Johnson, 1986; Fuge, 2013). The water content in the underthrust sediments decreases with increasing subduction depth and overburden pressure. Most of the pore water and bound water in hydrous minerals are expelled from the underthrust sediments before reaching the interplate seismogenic zone (Saffer et al., 2008; Kameda et al., 2011). Therefore, we assumed that a substantial portion of iodine in the underthrust sediments at the metagenesis to metamorphism stage is likely to exist as free molecular $I_2$.

To predict the physicochemical state of $I_2$ in the subduction zone, we compiled the phase diagram of $I_2$ under P–T conditions ranging from 0.01 to 3000 MPa and from 0 °C to 700 °C, as shown in Fig. 2A and B, using the available experimental data and empirical equations (Table S1). The melting curve between 250 and 1500 MPa was drawn based on the extrapolated curves obtained from laboratory experimental data (Babb Jr., 1969; Brazhkin et al., 1999) and Simon's equation, assuming it lies between the extrapolated curves above 250 MPa and below 1500 MPa (Fig. 2A). The experimental results in different laboratories are roughly consistent. The accuracy of the extrapolated melting curve is sufficient for the present study. The vapor pressure curve near the critical point, extrapolated from the experimental dataset (116.2 °C–263.2 °C) (Sako et al., 1979) and the Antoine equation (Table S2), showed a slight misalignment in pressure (approximately 1.2 MPa) at 546 °C. Thus, the vapor pressure curve was slightly adjusted to align with the critical point (Fig. 2A). The vapor pressure curve is drawn based on the experimental dataset and the Antoine equation, considering the triple and the critical points. As described later, the present study focuses mainly on the temperature area below 350 °C in the subduction zone. The accuracy of the vapor pressure curve in this temperature range is sufficient for the present study. However, there is still some uncertainty in this phase diagram, which requires improvement with additional experimental data. The phase diagram (Fig. 2B) reveals that $I_2$ primarily exists as a solid below 113 °C. As the temperature increases, the liquid phase of $I_2$ appears depending on the pressure. Owing to the partial pressure of $I_2$, some of it in the liquid phase may behave as a gas.

### 3.2. *P–T paths of the PAC and PHS on the $I_2$ phase diagram*

The Sanriku region in the Japan Trench and the Shikoku region in the

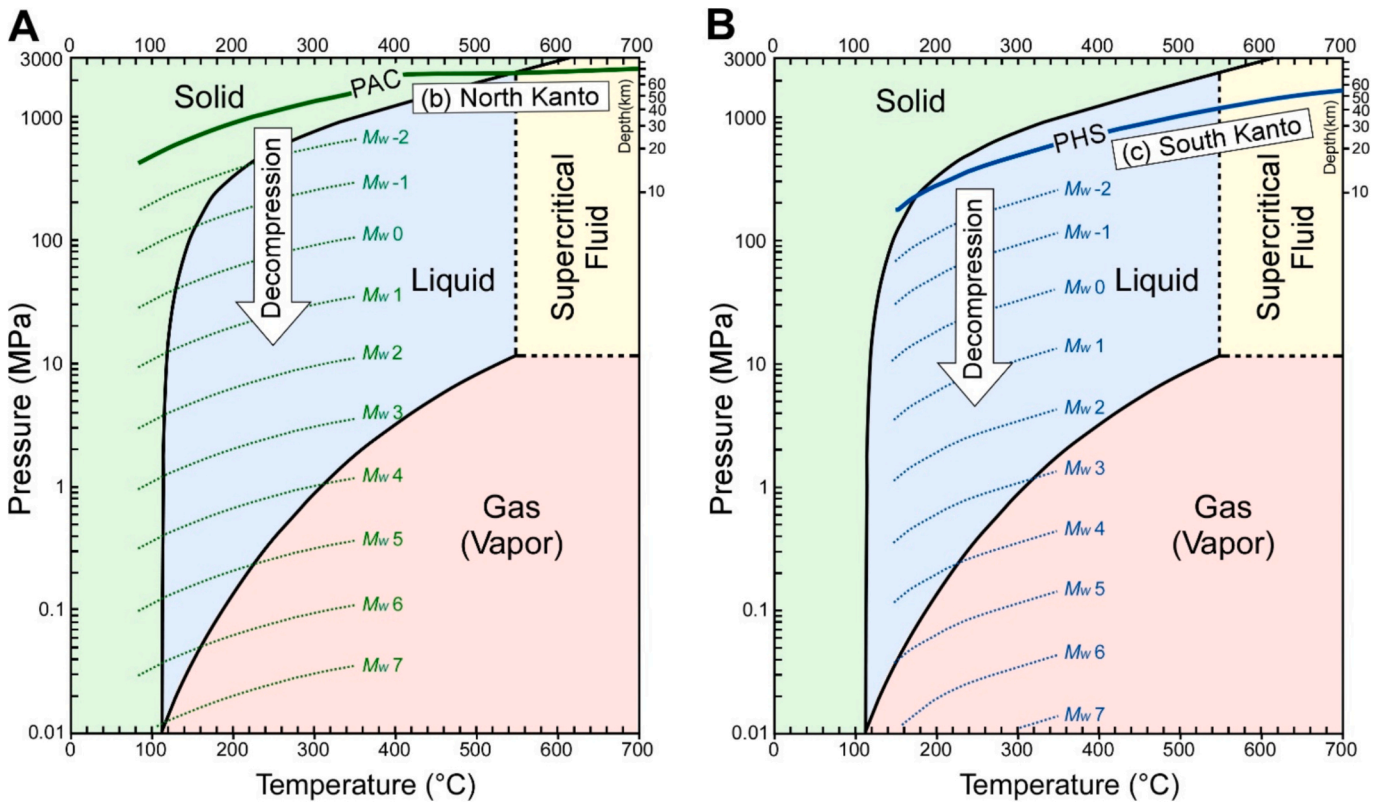


**Fig. 4.** Phase transitions of iodine owing to transient decompressions during earthquake ruptures. The transient decompressions from the P–T paths of (A) the PAC in (b) North Kanto and (B) the PHS in (c) South Kanto. The locations of (b) and (c) are shown in Fig. 3A and B, respectively. These transient decompressions in the subducted sediments were estimated using the piston model (Weatherley and Henley, 2013), which predicts the volume change in the fault jog caused by strike–slip fault displacement.

Nankai Trough are typical subduction zones for the PAC and PHS, respectively (Fig. 1). The P–T conditions at the surface of these oceanic plates in the Sanriku and Shikoku regions have been extensively studied (Peacock and Wang, 1999; Peacock, 2009). In the Kanto region, which contains $I_2$ deposits, the PHS subducts along the Sagami Trough, while the PAC subducts along the Japan Trench beneath the PHS slab (Fig. 1). Although the plate tectonic structure in the Kanto region is complex, 2D and 3D thermal modeling has been performed to clarify the thermal structure of the area (Yoshioka et al., 2015; Ji et al., 2017; Wada and He, 2017). In this study, we adopted the 3D thermal model of the Kanto region (Fig. 3A and B), which accounts for the effects of frictional heating and mantle wedge flows (Wada and He, 2017). This model, with a maximum decoupling depth of 75 km and an effective coefficient of friction of 0.03, aligns well with the observed distributions of heat flow and active volcanoes in and around the Kanto region. In this model, the down-dip limit of interplate seismicity on the PAC and PHS occurs around the 350 °C contour, which corresponds to the temperature at which the rheological transition from brittle to ductile behavior of the overlying crustal material controls seismicity (Hyndman and Wang, 1993; Wada and He, 2017).

The P–T paths at the surfaces of the PAC and PHS, as shown on the $I_2$ phase diagram, reveal a distinct difference (Fig. 3C). The younger PHS is comparatively warmer and has a smaller subduction angle than the older PAC (Peacock and Wang, 1999). Thus, the underthrust sediments subducting with the PHS experience higher temperatures and lower pressures than those associated with the PAC (Fig. 3C). The surface of the PHS in the (c) South Kanto region is at a higher temperature under the same pressure compared to the PHS in (d) Shikoku region owing to its proximity to the volcanic front (Figs. 1A and 3B). The surface of the PAC in the (b) North Kanto region is under higher temperature and lower pressure conditions than the PAC in the (a) Sanriku region (Fig. 3C), likely owing to the thermal interaction between the PAC and PHS in the Kanto region (Wada and He, 2017) (Fig. 3A). The P–T path of the underthrust sediments subducting with the PAC remains entirely in the solid region of $I_2$ (Fig. 3C). In contrast, when the temperature at the surface of the PHS exceeds approximately 160 °C, the P–T path enters the liquid region (Fig. 3C).

### 3.3. Flash vaporization of iodine in the subducted sediments

The subduction zone of the oceanic plate is an earthquake-prone region, where earthquake-induced rock destruction can expel gaseous substances such as thermogenic $CH_4$ and $H_2$ (Suzuki et al., 2024). Flash vaporization in earthquake rupture zones can also lead to the vaporization and expulsion of volatile substances, as well as the deposition of refractory materials (Weatherley and Henley, 2013). The extent of flash vaporization and expulsion of volatile substances during an earthquake rupture depends on the earthquake's moment magnitude ($M_w$). A simple piston model has been proposed to predict transient decompressions in fault jogs caused by the displacement of strike–slip faults during earthquakes (Weatherley and Henley, 2013). However, this model may not directly apply to predicting transient decompression in the rupture zones of interplate subduction earthquakes. However, it provides insight into the approximate relationship between $M_w$ and transient decompression during earthquake rupture. Because interplate subduction earthquakes occur at shallower depths than the down-dip limit of seismicity, the earthquake rupture zones in the PAC and PHS are located in a temperature range below 350 °C. The relationships between $M_w$ and transient decompression in this temperature range, based on the P–T paths of the PAC and PHS, are shown on the $I_2$ phase diagram (Fig. 4, Tables S3 and S4). As shown in Fig. 4A, when $M_w$ exceeds approximately 4, the $I_2$ phase transition from liquid to gas occurs during earthquake

rupture under the P–T conditions of the PAC in the (b) North Kanto region. Under the P–T conditions of the PHS in the (c) South Kanto region, when $M_w$ exceeds approximately 3, the liquid $I_2$ enters the gas-phase region (Fig. 4B). As a result, $I_2$ in the underthrust sediments of the PHS behaves as a vaporizable liquid from the outset, with vaporization occurring even at smaller $M_w$ compared to the PAC. Additionally, because the earthquake rupture zone in the PHS is at a shallower depth and lower pressure than in the PAC, the expulsion and subsequent secondary migration of $I_2$ in the PHS are more favorable than in the PAC. In subduction zones, the regional stress field may change throughout subduction earthquake cycles (Wang and Hu, 2006), and the above-mentioned argument could apply to normal-slip or strike–slip earthquakes, which commonly occur in the extensional stress field after a great earthquake (Lin et al., 2013). However, understanding the relationship between $M_w$ and transient decompression in the rupture zone during interplate subduction earthquakes remains a topic for future research.

The pore water in the subducted sediments at the interplate seismogenic zone is minimal (Saffer et al., 2008; Kameda et al., 2011). Even if some water is present, any dissolved $I_2$ and anions in the water are likely to flash-vaporize along with the water and free molecular $I_2$. The amount of iodine that flash-vaporizes from a single earthquake rupture may be limited. However, the interplate earthquakes occur highly frequently in the subduction zone. The frequency of earthquakes increases exponentially with a decrease in earthquake magnitude. In the Kanto subduction zone, the annual cumulative frequencies of earthquakes, by magnitude ($M$) based on seismograph readings from 1926 to 2010, are 1950 times ($M \geq 2$), 216 times ($M \geq 3$), 24 times ($M \geq 4$), and 3 times ($M \geq 5$), respectively (Nanjo et al., 2013). Frequent earthquakes can lead to a significant expulsion (primary migration) of iodine from the underthrust sediments.

### 3.4. Migration of iodine in the subduction zone

According to solubility thermodynamics (Ramette and Sandford Jr, 1965; Palmer et al., 1985), the relative abundance of dissolved iodine ($I_2$, $I^-$, and $I_3^-$) in water generally increases with temperature, suggesting that their secondary migration may be facilitated by deep fluids. Slab-dehydrated fluids are actively migrating through the décollement megathrust and splay faults in the Nankai Trough subduction zone

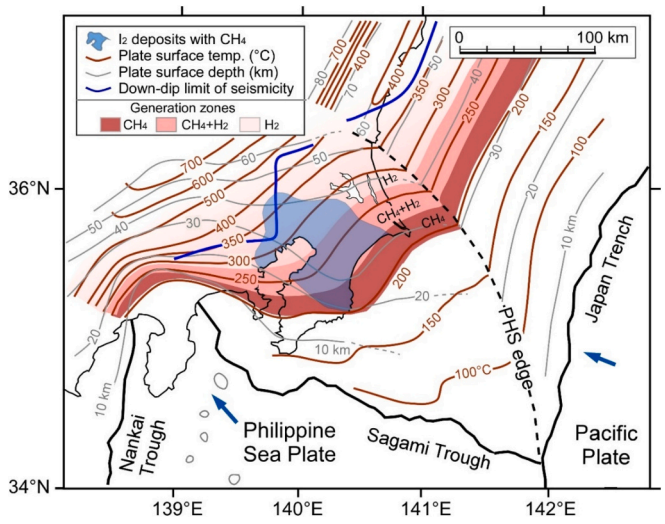


**Fig. 5.** Thermogenic $CH_4$ and $H_2$ generation zone of the underthrust sediments in the Kanto subduction zone. The temperatures of the thermogenic $CH_4$ and $H_2$ generation zones were estimated based on their maturity levels (Suzuki et al., 2024) and the heating rates of the underthrust sediments subducting with the PAC and PHS. The distribution of the PAC beneath the PHS is not shown.

(Saffer and Tobin, 2011; Wiersberg et al., 2018; Tsang et al., 2020; Tomonaga et al., 2020). These active deep fluids from the PHS can dissolve $I_2$, potentially promoting its upward migration. In contrast, in the subduction zone of the PAC, the migration of deep fluids appears to be less active because slab-dehydrated fluids are directed toward deep high-temperature zones, contributing to magma generation (Iwamori, 2000; Katayama, 2016). The volcanic front near the Kanto region is located along the PAC subduction zone (Fig. 1). However, the distribution of active volcanoes along the PHS subduction zone in the Kanto region is not distinct (Fig. 1), suggesting that the upward migration of slab-dehydrated fluids is active, similar to the Nankai Trough subduction zone. The more active upward migration of deep fluids in the PHS subduction zone compared to the PAC is likely attributed to slab dehydration occurring at lower pressures (shallower depths) and the slower subduction rate of the young, hot PHS (Katayama, 2016). The active upward migration of slab-dehydrated fluids from the PHS likely plays a crucial role in the long-distance transport of dissolved iodine. As discussed earlier, $I_2$ is more easily expelled from the subducted sediments of the PHS than those of the PAC. $I_2$ from the PHS likely plays a greater role in the formation of $I_2$ deposits in the South Kanto region. Hot springs and submarine seeps containing slab-dehydrated fluids in subduction zones are often rich in dissolved iodine (Muramatsu et al., 2001; Togo et al., 2020), supporting the idea that dissolved iodine is transported by deep fluids. However, because transporting dissolved iodine by deep fluids requires a large volume of fluid, gas-phase migration to aquifers is more efficient. $I_2$ has a high vapor pressure and readily sublimes. $I_2$, precipitated from deep fluids owing to a temperature drop during upward migration, could vaporize and migrate in the gas phase. However, our understanding of the migration of $I_2$ remains limited. Understanding the transportation of $I_2$ in the deep subsurface requires further study.

Muramatsu et al. (2001) concluded that the highly concentrated dissolved iodine in the aquifers of the South Kanto region primarily originated from sediments subducting with the PAC, based on the isotopic ages (40–50 Myr) of the dissolved iodine. This conclusion was made under the assumption that the mean geologic age of the PHS sediments around the Sagami Trough was 15 Myr. However, the geologic age of the PHS oceanic crust increases from the youngest part (~15 Myr) of the fossil spreading ridge near the Kii Peninsula to the South Kanto region, reaching approximately 50 Myr around the Sagami Trough (Hua et al., 2018). Furthermore, in previous iodine isotopic dating studies (Morane et al., 1998; Fehn et al., 2000; Muramatsu et al., 2001), the initial $^{129}I/^{127}I$ ratio was assumed to be $1.5 \times 10^{-12}$, a value now under debate. Recent research on $^{129}I$ dating (Ohta et al., 2024; Matsuzaki, 2024) suggests smaller initial $^{129}I/^{127}I$ ratios, which could considerably reduce the previously estimated iodine isotopic ages. These studies support the idea that the oceanic sediments subducting with the PHS are likely the primary source rocks for $I_2$ deposits in the South Kanto region.

### 3.5. Accumulation and coexistence of $I_2$ and $CH_4$

Microbial $CH_4$ produced by hydrogenotrophic methanogens is dissolved in the aquifers of the $I_2$ deposits (Kaneko et al., 2002; Mochimaru et al., 2007; Katayama et al., 2015), which requires a sufficient supply of $H_2$. In the subduction zone, thermogenic $H_2$ generated by the thermal decomposition of organic matter, mechanochemical $H_2$ from silicate rock fracturing, and $H_2$ derived from the serpentinization of ultramafic rocks can contribute to microbial $CH_4$ production (Suzuki et al., 2024). Both thermogenic and mechanochemical $H_2$ can be expelled alongside $I_2$ from the underthrust sediments during earthquake ruptures. Seismic attenuation analysis suggests the presence of a serpentinized mantle in the eastern PHS, near the boundary with the PAC (Nakajima, 2014). However, this serpentinization occurred before the subduction of the PHS in the Sagami Trough (Kamimura et al., 2002). Additional serpentinization of the PHS mantle after subduction may occur owing to slab-dehydrated fluids from the PAC (Nakajima, 2014), suggesting a

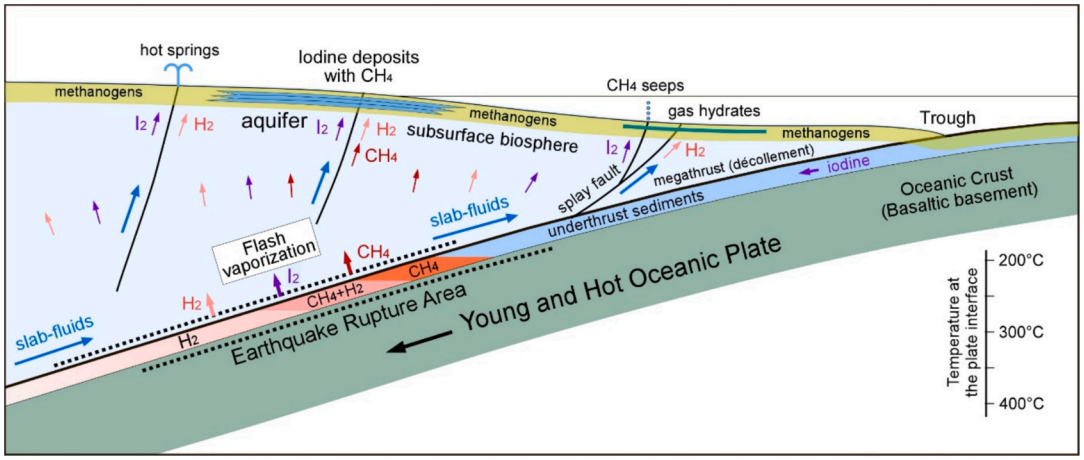


**Fig. 6.** Iodine expulsion, migration, and accumulation in the young and hot oceanic plate subduction zone. Various forms of iodine in the underthrust sediments subduct deep with the oceanic plate, remaining as molecular iodine ($I_2$) and undergoing metagenesis and metamorphism. In young, hot oceanic plates such as the PHS, $I_2$ in the underthrust sediments can behave as a liquid and undergo flash vaporization, being expelled owing to transient decompression caused by earthquake ruptures. Active slab-dehydrated fluids in the subduction zone of young, hot oceanic plates likely play a key role in transporting dissolved iodine ($I_2$, $I^-$, and $I_3^-$) to shallow subsurface aquifers. Because $I_2$ easily sublimes, some may migrate in the gas phase. The aquifer then acts as a trap and reservoir for migrating dissolved iodine. Thermogenic $CH_4$ and $H_2$ are also expelled from the underthrust sediments in the earthquake rupture zone and transported upward. $H_2$ that reaches the subsurface biosphere, particularly around shallow aquifers, contributes to microbial $CH_4$ production by hydrogenotrophic methanogens. The continuous supply of $I_2$ and $H_2$ from the subducted sediments to shallow aquifers in the subsurface biosphere leads to the formation of large-scale $I_2$ deposits alongside microbial $CH_4$. The aquifers may also contain a certain amount of thermogenic $CH_4$ from the underthrust sediments. The enrichment of $I_2$ and its coexistence with $CH_4$ in fluids, such as those in hot springs, submarine seeps, and gas hydrate water, is a result of the expulsion, migration, and accumulation of $I_2$, $CH_4$, and $H_2$ derived from the same underthrust sediments in the young and hot oceanic plate subduction zone.

potential $H_2$ supply near the boundary between the PAC and PHS. However, the upward migration of fluids from the PAC appears to be inactive (Iwamori, 2000; Katayama, 2016). Thermogenic $CH_4$ is also generated in the underthrust sediments at a maturity level close to the thermogenic $H_2$ generation stage (Li et al., 2017; Suzuki et al., 2017, 2024), which may contribute to the dissolved $CH_4$ in the aquifers of the $I_2$ deposits. We further investigated the spatial relationship between $I_2$ deposits and the thermogenic $CH_4$ and $H_2$ generation zones in the Kanto subduction zone.

The maturity levels of the thermogenic $CH_4$ and $H_2$ generation zones in organic-poor sediments correspond to vitrinite reflectance (VR) values of 1.5 %–4.5 % and > 2.5 %, respectively (Suzuki et al., 2024). The temperatures of these generation zones can be estimated using the kinetic model of VR, Easy%RoV (Burnham, 2019), considering the heating rate of subducted sediments. The heating rates for the PAC and PHS, estimated from their subduction rates and thermal structures, range from 50° to 200 °C $Myr^{-1}$ (Fig. 3A and B). The temperature ranges corresponding to VR values for the thermogenic $CH_4$ and $H_2$ generation zones at a heating rate of 50 °C $Myr^{-1}$ are 197 °C–272 °C and > 226 °C, respectively, while at 200 °C $Myr^{-1}$, they are 207 °C–283 °C and > 237 °C (Fig. S1, Table S5). Taking into account the difference in heating rate, the thermogenic $CH_4$ and $H_2$ generation zones in the PAC and PHS are estimated as shown in Fig. 5, with the generation zones in the PHS positioned almost directly beneath the $I_2$ deposits containing $CH_4$. The PAC subducting beneath the PHS likely plays an insufficient role in supplying $I_2$, thermogenic $CH_4$, and $H_2$ to the shallow aquifers, owing to the much deeper gas expulsion depth and the inactive upward migration of deep fluids. The thermogenic $CH_4$ and $H_2$ generation zone lies in the earthquake rupture area, suggesting that $I_2$ is expelled along with thermogenic $CH_4$ and $H_2$. These substances can be transported upward to the aquifers either by active deep fluids or through potential gas-phase migration.

The Kazusa Group, which intercalates large-scale aquifers, was formed 3–0.5 Myr ago by filling a trough-like basin (Kazusa Trough) created by tectonic activity around the triple plate junction, accompanied by a change in the PHS motion from north to northwest (Takahashi, 2006). The basin aquifers in the South Kanto region are primarily found in turbidite sandstones, and $I_2$ accumulation in these aquifers appears to have continued to the present (Kunisue et al., 2002; Mita et al., 2003). The $I_2$-concentrated aquifers have temperatures ranging from 23 °C to 40 °C (Kamei, 2001). Microbial $CH_4$ production likely occurs in or near these aquifers, where hydrogenotrophic methanogens can be highly active (Mochimaru et al., 2007; Katayama et al., 2015; Urai et al., 2021). $I_2$ and $H_2$ are expelled in a similar manner from the underthrust sediments subducting with the PHS and are continuously supplied to the aquifers, likely resulting in the coexistence of $I_2$ and microbial $CH_4$. The carbon isotope composition ($\delta^{13}C$ value) of $CH_4$ from the South Kanto gas field ranges from −68 ‰ to −60 ‰ (Igari and Sakata, 1989; Kaneko et al., 2002; Katayama et al., 2015). These values are relatively high for primary microbial $CH_4$ produced by hydrogenotrophic methanogens, suggesting a mix of thermogenic and microbial $CH_4$ (Whiticar, 1999; Milkov and Etiope, 2018). Natural gas emitted from the fault zone in the South Kanto region contains $^{13}C$-rich thermogenic $CH_4$ ($\delta^{13}C = -36.3$ ‰) (Nakata et al., 2012), supporting the contribution of thermogenic $CH_4$ to the aquifers of $I_2$ deposits. Compared to the sedimentary rocks in the Kanto Basin, the underthrust sediments of the PHS are subducting at a considerably higher rate along with the oceanic plate, having moved approximately 100 km through the interplate seismogenic zone since the deposition of the Kazusa Group 3 Myr ago. Substantial amounts of $I_2$, $CH_4$, and $H_2$ have likely been expelled from the underthrust sediments subducting with the young and hot PHS, contributing to the formation of large-scale $I_2$ deposits alongside microbial and thermogenic $CH_4$.

The high concentrations of iodine, ranging from 0.5 to 2 mM, have been found in $CH_4$ gas hydrate waters from the oceanic plate subduction zones in the Nankai Trough, Cascadia Margin, Peru Margin, and Costa Rica Margin (Fehn et al., 2007; Fehn, 2012). In these earthquake-prone subduction zones, young oceanic plates, the PHS, the Juan de Fuca Plate, the Nazca Plate, and the Cocos Plate, that formed during and after the Paleogene, are currently subducting, respectively (Wilson, 1988; Von Huene and Lallemand, 1990; Lonsdale, 2005; Seton et al., 2020). The P–T conditions of the interplate seismogenic zone in these subduction zones appear to be lower pressure and higher temperature compared to the old PAC, similar to the PHS (Hyndman and Wang, 1993; Harris and Wang, 2002; Leite Neto et al., 2024). Coexistence and enrichment of $I_2$

and $CH_4$ in fluids in these subduction zones of young and hot oceanic plates also suggest that the P–T conditions of the oceanic plate significantly influence the expulsion and migration of $I_2$ and $CH_4$ in the forearc areas.

## 4. Conclusion

The behavior of $I_2$ in the subduction zone of a young and hot oceanic plate is summarized in Fig. 6. In this subduction system, the sediments subducting with the oceanic plate experience lower pressure and higher temperature conditions, while slab-dehydrated fluids remain active. The $I_2$ in the subducted sediments can exist as a liquid, leading to its flash vaporization during earthquake ruptures, even with a small moment magnitude. The expelled $I_2$, likely along with thermogenic $CH_4$ and $H_2$ from the subducted sediments, can then migrate upward with the active slab-dehydrated fluids, contributing to the formation of $I_2$ deposits containing $CH_4$ in the aquifers. The high concentrations of $I_2$ and $CH_4$ found in hot springs, submarine seeps, and gas hydrate waters in the subduction zone of the PHS can be explained similarly (Fig. 6). In the Kanto subduction zone, tectonic activity around the triple plate junction, along with a change in the direction of PHS motion, led to the formation of the Kazusa Group. This Group intercalates a vast aquifer that has served as a trap and reservoir for dissolved iodine and $CH_4$ ever since. The development of large-scale $I_2$ deposits with $CH_4$ in the South Kanto region is attributed to the geological formation of this extensive aquifer directly above the expulsion zone of $I_2$, $CH_4$, and $H_2$ in the underthrust sediments subducting with the young and hot PHS. Coexistence and enrichment of $I_2$ and $CH_4$ in crustal fluids at other subduction zones may be explained similarly, as due to the expulsion and migration of $I_2$, $CH_4$, and $H_2$ from the oceanic sediments subducting with the young and hot oceanic plates.

## CRediT authorship contribution statement

**Noriyuki Suzuki:** Writing – review & editing, Writing – original draft, Visualization, Supervision, Project administration, Methodology, Investigation, Funding acquisition, Formal analysis, Conceptualization. **Jun Kameda:** Writing – review & editing, Validation, Methodology, Investigation. **Miki Amo:** Writing – review & editing, Validation, Funding acquisition.

## Declaration of competing interest

The authors declare that they have no known competing financial interests or personal relationships that could have appeared to influence the work reported in this paper.

## Acknowledgments

The authors are grateful to Dr. Yi-Xiang Chen and anonymous reviewers for their valuable and constructive comments on the manuscript. The authors also appreciate the Japan Organization for Metals and Energy Security (JOGMEC) for their support in publishing this paper. This research is supported by Japan Society for the Promotion of Science (JSPS) Grant-in-Aid for Scientific Research 21K03712 to NS.

## Appendix A. Supplementary data

Supplementary data to this article can be found online at https://doi.org/10.1016/j.chemgeo.2025.123031.

## Data availability

Data will be made available on request.

## References

Babb Jr., S.E., 1969. Melting curves of volatile materials. J. Chem. Phys. 50, 5271–5274. https://doi.org/10.1063/1.1671045.

Brazhkin, V.V., Popova, S.V., Voloshin, R.N., 1999. Pressure–temperature phase diagram of molten elements: selenium, sulfur and iodine. Phys. B Condens. Matter 265 (1–4), 64–71. https://doi.org/10.1016/S0921-4526(98)01318-0.

Burnham, A.K., 2019. Kinetic models of vitrinite, kerogen, and bitumen reflectance. Org. Geochem. 131, 50–59. https://doi.org/10.1016/j.orggeochem.2019.03.007.

Cosgrove, M.E., 1970. Iodine in the bituminous Kimmeridge shales of the Dorset Coast, England. Geochim. Cosmochim. Acta 34, 830–836. https://doi.org/10.1016/0016-7037(70)90033-5.

Fehn, U., 2012. Tracing crustal fluids: applications of Natural $^{129}I$ and $^{36}Cl$. Annu. Rev. Earth Planet. Sci. 40, 45–67. https://doi.org/10.1146/annurev-earth-042711-105528.

Fehn, U., Snyder, G., Egeberg, P.K., 2000. Dating of pore waters with $^{129}I$: Relevance for the origin of marine gas hydrates. Science 289, 2332–2335. https://doi.org/10.1126/science.289.5488.2332.

Fehn, U., Snyder, G.T., Matsumoto, R., Muramatsu, Y., Tomaru, H., 2003. Iodine dating of pore waters associated with gas hydrates in the Nankai area, Japan. Geology 31, 521–524. https://doi.org/10.1130/0091-7613(2003)031<0521:IDOPWA>2.0.CO;2.

Fehn, U., Lu, Z., Tomaru, H., 2006. Data report: $^{129}I/I$ ratios and halogen concentrations in pore water of hydrate ridge and their relevance for the origin of gas hydrates: a progress report. Proc. ODP Sci. Results 204, 1–25. http://www-odp.tamu.edu/publications/204_SR/VOLUME/CHAPTERS/107.PDF.

Fehn, U., Snyder, G.T., Muramatsu, Y., 2007. Iodine as a tracer of organic material: $^{129}I$ results from gas hydrate systems and fore arc fluids. J. Geochem. Explor. 95, 66–80. https://doi.org/10.1016/j.gexplo.2007.05.005.

Fuge, R., 2013. Soils and iodine deficiency. In: Selinus, O. (Ed.), Essentials of Medical Geology, Revised edition. Springer, Dordrecht, pp. 417–432. https://doi.org/10.1007/978-94-007-4375-5_17.

Fuge, R., Johnson, C.C., 1986. The geochemistry of iodine – a review. Environ. Geochem. Health 8, 31–54. https://doi.org/10.1007/BF02311063.

Geological Survey of Japan, AIST, 2023. Seamless Digital Geological Map of Japan V2 1: 200,000, Original Edition. https://gbank.gsj.jp/seamless/ [Accessed: Mar. 3rd, 2025].

Harris, R.N., Wang, K., 2002. Thermal models of the middle America Trench at the Nicoya Peninsula, Costa Rica. Geophys. Res. Lett. 29, 2010. https://doi.org/10.1029/2002GL015406.

Harvey, G.R., 1980. A study of the chemistry of iodine and bromine in marine sediments. Mar. Chem. 8, 327–332. https://doi.org/10.1016/0304-4203(80)90021-3.

Hua, Y., Zhao, D., Xu, Y., Liu, X., 2018. Age of the subducting Philippine Sea slab and mechanism of low-frequency earthquakes. Geophys. Res. Lett. 45, 2303–2310. https://doi.org/10.1002/2017GL076531.

Hyndman, R.D., Wang, K., 1993. Thermal constrains on the zone of major thrust failure: the Cascadia Subduction Zone. J. Geophys. Res. 98, 2039–2060. https://doi.org/10.1029/92JB02279.

Igari, S., Sakata, S., 1989. Origin of natural gas of dissolved-in water type in Japan inferred from chemical and isotopic compositions: Occurrence of dissolved gas of thermogenic origin. Geochem. J. 23, 139–142. https://doi.org/10.2343/geochemj.23.139.

Iwamori, H., 2000. Deep subduction of $H_2O$ and deflection of volcanic chain towards backarc near triple junction due to lower temperature. Earth Planet. Sci. Lett. 181, 41–46. https://doi.org/10.1016/S0012-821X(00)00180-1.

Ji, Y., Yoshioka, S., Manea, V.C., Manea, M., Matsumoto, T., 2017. Three-dimensional numerical modeling of thermal regime and slab dehydration beneath Kanto and Tohoku, Japan. J. Geophys. Res. Solid Earth 122, 332–353. https://doi.org/10.1002/2016JB013230.

JNGA (Japan Natural Gas Association), 2024. Overview of Natural Gas of Dissolved-in-Water Type in Chiba Prefecture. https://www.tengas.gr.jp/keiyo/keiyo_outline/.

Kameda, J., Yamaguchi, A., Saito, S., Sakuma, H., Kawamura, K., Kimura, G., 2011. A new source of water in seismogenic subduction zones. Geophys. Res. Lett. 38, L22306. https://doi.org/10.1029/2011GL048883.

Kamei, G., 2001. The source and behavior of iodine dissolving in groundwater in the Mobara gas field. Resour. Geol. 51, 145–151. https://doi.org/10.11456/shigenchishitsu1992.51.145.

Kamimura, A., Kasahara, J., Shinohara, M., Hino, R., Shiobara, H., Fujie, G., Kanazawa, T., 2002. Crustal structure study at the Izu-Bonin subduction zone around 31°N: implications of serpentinized materials along the subduction plate boundary. Phys. Earrth Planet. Inter. 132, 105–129. https://doi.org/10.1016/S0031-9201(02)00047-X.

Kaneko, N., Maekawa, T., Igari, S., 2002. Generation of archaeal methane and its accumulation mechanism into interstitial water. J. Jap. Assoc. Petrol. Tech. 67, 97–110. https://doi.org/10.3720/japt.67.1_97.

Katayama, I., 2016. Water circulation system at subduction zones. Bull. Volc. Soc. Jpn. 61, 69–77. https://doi.org/10.18940/kazan.61.1_69.

Katayama, T., Yoshioka, H., Muramoto, Y., Usami, J., Fujiwara, K., Yoshida, S., Kamagata, Y., Sakata, S., 2015. Physicochemical impacts associated with natural gas development on methanogenesis in deep sand aquifers. ISME J. 9, 436–446. https://doi.org/10.1038/ismej.2014.140.

Koma, T., Suzuki, Y., Kodama, K., 1983. Forms of sulfur, carbon, chlorine and iron compounds and their depositional environment, in the Kazusa Group, the Boso Peninsula, Central Japan. Bull. Geol. Surv. Japan 34, 191–206. https://www.gsj.jp/data/bull-gsj/34-04_04.pdf.

Kunisue, S., Mita, I., Waki, F., 2002. Relationship between subsurface geology and productivity of natural gas and iodine in the Mobara gas field, Boso Peninsula, Central Japan. J. Jap. Assoc. Petrol. Tech. 67, 83–96. https://doi.org/10.3720/japt.67.1_83.

Leite Neto, G.S., Julià, J., Prieto, G.A., 2024. Deep-focus earthquake mechanism at the subducting Nazca plate (Peru-Brazil Border): cold slab behovior in a warm plate. Earth Space Sci. 11. https://doi.org/10.1029/2024EA003617 e2024EA003617.

Leonard, M., 2014. Self-consistent earthquake fault-scaling relations: update and extension to stable continental strike-slip faults. Bull. Seismol. Soc. Am. 104, 2953–2965. https://doi.org/10.1785/0120140087.

Li, X., Krooss, B.M., Weniger, P., Littke, R., 2017. Molecular hydrogen ($H_2$) and light hydrocarbon gases generation from marine and lacustrine source rocks during closed-system laboratory pyrolysis experiments. J. Anal. Appl. Pyrolysis 126, 275–287. https://doi.org/10.1016/j.jaap.2017.05.019.

Lin, W., Conin, M., Moore, J.C., Chester, F.M., Nakamura, Y., Mori, J.J., Anderson, L., Brodsky, E.E., Eguchi, N., Expedition 343 Scientists, Cook, B., Jeppson, T., Wolfson-Schwehr, M., Sanada, Y., Saito, S., Kido, Y., Hirose, T., Behrmann, J.H., Ikari, M., Ujiie, K., Rowe, C., Kirkpatrick, J., Bose, S., Regalla, C., Remitti, F., Toy, V., Fulton, P., Mishima, T., Yang, T., Sun, T., Ishikawa, T., Sample, J., Takai, K., Kameda, J., Toczko, S., Maeda, L., Kodaira, S., Hino, R., Saffer, D., 2013. Stress state in the largest displacement area of the 2011 Tohoku-Oki earthquake. Science 339, 687–690. https://doi.org/10.1126/science.1229379.

Lonsdale, P., 2005. Creation of the Cocos and Nazca plates by fission of the Farallon plate. Tectonophysics 404, 237–264. https://doi.org/10.1016/j.tecto.2005.05.011.

Matsuzaki, H., 2024. Decoding the time information by the analysis of isotope system Iodine-129, a potential dating tool. Radioisotopes 73, 47–59. https://doi.org/10.3769/radioisotopes.73.47.

Milkov, A.V., Etiope, G., 2018. Revised genetic diagrams for natural gases based on a global dataset of >20,000 samples. Org. Geochem. 125, 109–120. https://doi.org/10.1016/j.orggeochem.2018.09.002.

Mita, I., Waki, F., Kunisue, S., 2003. Control factors on gas-water ratio and iodine concentration around the Kujukuri District in Chiba Prefecture, central Japan–Special reference to the role of submarine fan deposits and faults in the Kazusa Group. J. Jap. Assoc. Petrol. Tech. 68, 111–123. https://doi.org/10.3720/japt.68.111.

Mochimaru, H., Uchiyama, H., Yoshioka, H., Imachi, H., Hoaki, T., Tamaki, H., Nakamura, K., Sekiguchi, Y., Kamagata, Y., 2007. Methanogen diversity in deep subsurface gas-associated water at the Minami-Kanto gas field in Japan. Geomicrobiol J. 24, 93–100. https://doi.org/10.1080/01490450701266571.

Morane, J.E., Fehn, U., Teng, R.T.D., 1998. Variations in $^{129}I/^{127}I$ ratios in recent marine sediments: evidence for a fossil organic component. Chem. Geol. 152, 193–203. https://doi.org/10.1016/S0009-2541(98)00106-5.

Muramatsu, Y., Wedepohl, K.H., 1998. The distribution of iodine in the earth's crust. Chem. Geol. 147, 201–216. https://doi.org/10.1016/S0009-2541(98)00013-8.

Muramatsu, Y., Fehn, U., Yoshida, S., 2001. Recycling of iodine in fore-arc areas: evidence from the iodine brines in Chiba, Japan. Earth Planet. Sci. Lett. 192, 583–593. https://doi.org/10.1016/S0012-821X(01)00483-6.

Nakajima, J., 2014. Seismic attenuation beneath Kanto, Japan: evidence for high attenuation in the serpentinized subducting mantle. Earth Pl. Sp. 66, 12. https://doi.org/10.1186/1880-5981-66-12.

Nakata, E., Tanaka, S., Suenaga, H., Mahara, Y., Nakamura, T., Nakagawa, K., Ohta, T., 2012. Stable carbon isotope behaviour of natural seepage of deep underground $^{13}C$-rich methane detected along a fault zone and adsorbed in mudstone: Tokyo Bay area, Japan. Appl. Geochem. 27, 1710–1723. https://doi.org/10.1016/j.apgeochem.2012.02.007.

Nanjo, K.Z., Sakai, S., Kato, A., Tsuruoka, H., Hirata, N., 2013. Time-dependent earthquake probability calculations for southern Kanto after the 2011 *M*9.0 Tohoku earthquake. Geophys. J. Int. 914–919. https://doi.org/10.1093/gji/ggt009.

Ohta, T., Hasegawa, T., Jiang, W., Yang, G.M., Lu, Z.T., Mahara, Y., 2024. Feasibility of $^{129}I$ groundwater dating calibrated by both $^{81}Kr$ and $^{4}He$ for the assessment of deep geological repositories in Japan. Sci. Rep. 14, 15688. https://doi.org/10.1038/s41598-024-66250-3.

Palmer, D.A., Ramette, R.W., Mesmer, R.E., 1985. The hydrolysis of iodine: Equilibria at high temperatures. J. Nuclear Mat. 130, 280–286. https://doi.org/10.1016/0022-3115(85)90317-4.

Pavese, F., 2022. The triple point temperature of iodine. J. Chem. Thermodyn. 165, 106639. https://doi.org/10.1016/j.jct.2021.106639.

Peacock, S.M., 2009. Thermal and metamorphic environment of subduction zone episodic tremor and slip. J. Geophys. Res. 114, B00A07. https://doi.org/10.1029/2008JB005978.

Peacock, S.M., Wang, K., 1999. Seismic consequences of warm versus cool subduction metamorphism: examples from southwest and Northeast Japan. Science 286, 937–939. https://doi.org/10.1126/science.286.5441.937.

Pepper, A.S., 1991. Estimating the petroleum expulsion behaviour of source rocks: a novel quantitative approach. Geol. Soc. Lond. Spec. Publ. 59, 9–31. https://doi.org/10.1144/GSL.SP.1991.059.01.0.

Price, N.B., Calvert, S.E., 1977. The contrasting geochemical behaviours of iodine and bromine in recent sediments from the Namibian shelf. Geochim. Cosmochim. Acta 41, 1769–1775. https://doi.org/10.1016/0016-7037(77)90209-5.

Raimbourg, H., Thiery, R., Vacelet, M., Famin, V., Ramboz, C., Boussafir, M., Disnar, J.R., Yamaguchi, A., 2017. Organic matter cracking: a source of fluid overpressure in subducting sediments. Tectonophys 721, 245–274. https://doi.org/10.1016/j.tecto.2017.08.005.

Ramette, R.W., Sandford Jr., R.W., 1965. Thermodynamics of iodine solubility and triiodide ion formation in water and deuterium oxide. J. Amer. Chem. Soc. 87, 5001–5005. https://doi.org/10.1021/ja00950a005.

Saffer, D.M., Tobin, H., 2011. Hydrogeology and mechanics of subduction zone forearcs: fluid flow and pore pressure. Annu. Rev. Earth Planet. Sci. 39, 157–186. https://doi.org/10.1146/annurev-earth-040610-133408.

Saffer, D.M., Underwood, M.B., McKiernan, A.W., 2008. Evaluation of factors controlling smectite transformation and fluid production in subduction zones: Application to the Nankai Trough. Island Arc 17, 208–230. https://doi.org/10.1111/j.1440-1738.2008.00614.x.

Sako, T., Haraya, K., Shindo, Y., Obata, K., Hakuta, T., 1979. Vapor pressure of liquid iodine. Kagaku Kogaku Ronbunshu 5, 304–307. https://doi.org/10.1252/kakoronbunshu.5.304.

Sanchez-Alfaro, P., Reich, M., Driesner, T., Cembrano, J., Arancibia, G., Perez-Flores, P., Heinrich, C.A., Rowland, J., Tardani, D., Lange, D., Campos, E., 2016. The optimal windows for seismically-enhanced gold precipitation in the epithermal environment. Ore Geol. Rev. 79, 463–473. https://doi.org/10.1016/j.oregeorev.2016.06.005.

Sawaki, T., Kaneko, N., Maekawa, T., Igari, S., 2016. Fuel resource map "Kanto Region". GSJ Chishitsu News 5, 45–49. https://www.gsj.jp/data/gcn/gsj_cn_vol5.no2_45-49.pdf.

Schnebele, E.K., 2024. Iodine, U.S. Geological Survey, Mineral Commodity Summaries, January 2024. https://pubs.usgs.gov/periodicals/mcs2024/mcs2024-iodine.pdf.

Seton, M., Müller, R.D., Zahirovic, S., Williams, S., Wright, N.M., Cannon, J., Whittaker, J.M., Matthews, K.J., McGirr, R., 2020. A global data set of present-day oceanic crustal age and seafloor spreading parameters. Geochem. Geophys. Geosyst. 21. https://doi.org/10.1029/2020GC009214 e2020GC009214.

Suzuki, N., Saito, H., Hoshino, T., 2017. Hydrogen gas of organic origin in shales and metapelites. Int. J. Coal Geol. 173, 227–236. https://doi.org/10.1016/j.coal.2017.02.014.

Suzuki, N., Koike, K., Kameda, J., Kimura, G., 2024. Thermogenic methane and hydrogen generation in subducted sediments of the Nankai Trough. Commn. Earth Environ. 5, 97. https://doi.org/10.1038/s43247-024-01252-7.

Takahashi, M., 2006. Tectonic development of the Japanese Islands controlled by Philippine Sea Plate motion. J. Geogr. 115, 116123. https://doi.org/10.5026/jgeography.115.116.

Tissot, B.P., Welte, D.H., 2013. Petroleum Formation and Occurrence. Second Revised and Enlarged Edition. Springer Science & Business Media, p. 702.

Togo, Y.S., Kazahaya, K., Tosaki, Y., Takahashi, M., Morikawa, N., Takahashi, H.A., Nakamura, Y., Inamura, A., Shimizu, H., Matsuzaki, H., 2020. Detection of slab-derived fluid in coastal area of Seto Inland Sea Japan based on $^{129}I/^{127}I$ ratios and halogen composition. Chikyukagaku (Geochem.) 54, 189–200. https://doi.org/10.14934/chikyukagaku.54.189.

Tomaru, H., Lu, Z., Fehn, U., Muramatsu, Y., Matsumoto, R., 2007. Age variation of pore water iodine in the eastern Nankai Trough, Japan: evidence for different methane sources in a large gas hydrate field. Geology 35, 1015–1018. https://doi.org/10.1130/G24198A.1.

Tomaru, H., Lu, Z., Fehn, U., Muramatsu, Y., 2009. Origin of hydrocarbons in the Green Tuff region of Japan: $^{129}I$ results from oil field brines and hot springs in the Akita and Niigata Basins. Chem. Geol. 264, 221–231. https://doi.org/10.1016/j.chemgeo.2009.03.008.

Tomonaga, Y., Yagasaki, K., Park, J.O., Ashi, J., Toyoda, S., Takahata, N., Sano, Y., 2020. Fluid dynamics along the Nankai Trough: He isotopes reveal direct seafloor mantle-fluid emission in the Kumano basin (Southwest Japan). ACS Earth Space Chem. 4, 2105–2112. https://doi.org/10.1021/acsearthspacechem.0c00229.

Tsang, M.Y., Bowden, S.A., Wang, Z., Mohammed, A., Tonai, S., Muirhead, D., Yang, K., Yamamoto, Y., Kamiya, N., Okutsu, N., Hirose, T., Kars, M., Schubotz, F., Ijiri, A., Yamada, Y., Kubo, Y., Morono, Y., Inagaki, F., Heuer, V.B., Hinrichs, K.U., 2020. Hot fluids, burial metamorphism and thermal histories in the underthrust sediments at IODP 370 site C0023, Nankai Accretionary Complex. Mar. Pet. Geol. 112, 104080. https://doi.org/10.1016/j.marpetgeo.2019.104080.

Tsunogai, S., Henmi, T., 1971. Iodine in the surface water of the ocean. J. Oceano. Soc. Japan 27, 67–72. https://doi.org/10.1007/BF02109332.

Ungerer, P., 1990. State of the art of research in kinetic modelling of oil formation and expulsion. Org. Geochem. 16, 1–25. https://doi.org/10.1016/0146-6380(90)90022-R.

Urai, A., Takano, Y., Imachi, H., Ishii, S., Matsui, Y., Ogawara, M., Tasumi, E., Miyairi, Y., Ogawa, N.O., Yoshimura, T., Inagaki, F., Yokoyama, Y., Kawano, K., Murai, D., Park, H.D., Ohkouchi, N., 2021. Origin of deep methane associated with a unique community of microorganisms in an organic- and iodine-rich aquifer. ACS Earth Space Chem. 5, 1–11. https://doi.org/10.1021/acsearthspacechem.0c00204.

Von Huene, R., Lallemand, S., 1990. Tectonic erosion along the Japan and Peru convergent margins. Geol. Soc. Am. Bull. 102, 704–720. https://doi.org/10.1130/0016-7606(1990)102<0704:TEATJA>2.3.CO;2.

Wada, I., He, J., 2017. Thermal structure of the Kanto region, Japan. Geophys. Res. Lett. 44, 7194–7202. https://doi.org/10.1002/2017GL073597.

Wang, K., Hu, Y., 2006. Accretionary prisms in subduction earthquake cycles: the theory of dynamic Coulomb wedge. J. Geophys. Res. 111, B06410. https://doi.org/10.1029/2005JB004094.

Weatherley, D.K., Henley, R.W., 2013. Flash vaporization during earthquakes evidenced by gold deposits. Nat. Geosci. 6, 294–298. https://www.nature.com/articles/ngeo1759.

Whiticar, M.J., 1999. Carbon and hydrogen isotope systematics of bacterial formation and oxidation of methane. Chem. Geol. 161, 291–314. https://doi.org/10.1016/S0009-2541(99)00092-3.

Wiersberg, T., Hammerschmidt, S.B., Fuchida, S., Kopf, A., Erzinger, J., 2018. Mantle-derived fluids in the Nankai Trough Kumano forearc basin. Prog. Earth Planet Sci. 5, 79. https://doi.org/10.1186/s40645-018-0235-0.

Wilson, D.S., 1988. Tectonic history of the Juan de Fuca Ridge over the last 40 million years. J. Geophys. Res. 93, 11863–11867. https://doi.org/10.1029/JB093iB10p11863.

Yonetani, H., Koma, T., Suzuki, Y., Kodama, K., 1983. The distribution of organic carbon and *n*-paraffine in the Kazusa, Miura and Hota groups in the Boso Peninsula, Central Japan. Bull. Geol. Surv. Japan 34, 153–174. https://www.gsj.jp/data/bull-gsj/34-04_01.pdf.

Yoshioka, S., Takagi, R., Matsumoto, T., 2015. Relationship between temperatures and fault slips on the upper surface of the sbducting Philippine Sea plate beneath the Kanto district, Central Japan. Geophys. J. Int. 201, 878–890. https://doi.org/10.1093/gji/ggv032.